DE GRUYTER

Chemical Papers 69 (1) 134–142 (2015)
DOI: 10.1515/chempap-2015-0004

ORIGINAL PAPER

Electrochemical nanostructured biosensors: carbon nanotubes versus conductive and semi-conductive nanoparticles

[a]Nima Aliakbarinodehi*, [a]Irene Taurino, [b]Jagdale Pravin, [b]Alberto Tagliaferro, [c]Gianluca Piccinini, [a]Giovanni De Micheli, [a]Sandro Carrara

[a]*Integrated Systems Laboratory, École Polytechnique Fédérale de Lausanne (EPFL), Route Cantonale, 1015 Lausanne, Switzerland*

[b]*Department of Applied Science and Technology,* [c]*Department of Electronics and Telecommunications, Politecnico di Torino, Corso Duca degli Abruzzi, 24, 10129 Torino, Italy*

Received 13 March 2014; Revised 26 June 2014; Accepted 30 June 2014

The aim of this work was to demonstrate that various types of nanostructures provide different gains in terms of sensitivity or detection limit albeit providing the same gain in terms of increased area. Commercial screen printed electrodes (SPEs) were functionalized with 100 μg of bismuth oxide nanoparticles (Bi_2O_3 NPs), 13.5 μg of gold nanoparticles (Au NPs), and 4.8 μg of multi-wall carbon nanotubes (MWCNTs) to sense hydrogen peroxide (H_2O_2). The amount of nanomaterials to deposit was calculated using specific surface area (SSA) in order to equalize the additional electroactive surface area. Cyclic voltammetry (CV) experiments revealed oxidation peaks of Bi_2O_3 NPs, Au NPs, and MWCNTs based electrodes at (790 ± 1) mV, (386 ± 1) mV, and (589 ± 1) mV, respectively, and sensitivities evaluated by chronoamperometry (CA) were (74 ± 12) μA mM^{-1} cm^{-2}, (129 ± 15) μA mM^{-1} cm^{-2}, and (54 ± 2) μA mM^{-1} cm^{-2}, respectively. Electrodes functionalized with Au NPs showed better sensing performance and lower redox potential (oxidative peak position) compared with the other two types of nanostructured SPEs. Interestingly, the average size of the tested Au NPs was 4 nm, under the limit of 10 nm where the quantum effects are dominant. The limit of detection (LOD) was (11.1 ± 2.8) μM, (8.0 ± 2.4) μM, and (3.4 ± 0.1) μM for Bi_2O_3 NPs, Au NPs, and for MWCNTs based electrodes, respectively.

Keywords: multi-wall carbon nanotube, cyclic voltammetry, chronoamperometry, hydrogen peroxide, bismuth oxide nanoparticle, gold nanoparticle

Introduction

Low-cost, simple, efficient, and highly sensitive electrochemical biosensors are attractive for the detection and quantification of many compounds. Here, the performance of different nanostructured SPEs in H_2O_2 sensing is investigated, since this compound is involved in oxidase-based sensing and thus, it is a key element in the analysis of various organic compounds and enzymatic reactions (Boero et al., 2011; Wang & Hu, 2009; Pumera et al., 2007). In this work, the oxidation peak of H_2O_2 is determined by CV experiments, and the applied potential of CA is set slightly beyond this value to examine the performance of the functionalized SPEs against H_2O_2.

Many novel nanostructures enhancing the electron transfer rate between electrodes and targets and thus increasing the performance of the devices have been developed and exploited. Electrochemical and optical properties of semiconductor nanoparticles (NPs) are tunable with their size; a well-known example of this being the blue shift in the absorption edge of NPs while decreasing their size (Trindade et al., 2001). Size dependent properties are the result of high fraction of

*Corresponding author, e-mail: Nima.aliakbarinodehi@epfl.ch, Nima.aliakbari@gmail.com

surface atoms and quantum effects (Alivisatos, 1996). Many applications in electronics (Ding et al., 2006; Liu et al., 2012), catalysis and sensing (Bredol & Kaczmarek, 2010; Willner et al., 2007), solar-energy conversion (Jiang et al., 2013; Guo et al., 2013), optoelectronics (Zeng et al., 2010; Kairdolf et al., 2013), quantum devices (Pumera et al., 2007), and single electron transistors (Facci et al., 1996) take advantage of the particle size tuning. Bi_2O_3 NPs (Zhang et al., 2010; Ge et al., 2011) provide enhanced catalytic and electrochemical activity compared to their bulk counterpart (Shipway & Willner, 2001), which is induced by the high surface/volume ratio, high defect concentration on surface (porous morphology), and the unique electronic properties (Zhang, 1997; Banks et al., 2005). These properties as well as the nontoxic nature and biocompatibility make Bi_2O_3 NPs a suitable choice for biosensing applications (Periasamy et al., 2011).

Conductivity and nanoscale dimensions of metal NPs (mostly Au NPs) were employed in many enzymatic (Pingarrón et al., 2008; Shumyantseva et al., 2005) and non-enzymatic (Wang & Zheng, 2010; Yin et al., 2014) biosensing applications. Metal NPs have been deposited on a wide range of substrates by electrodeposition (Wang & Zheng, 2010), self-assembly (Nie et al., 2010; Sun, 2006) and precipitation (Shumyantseva et al., 2005; Guascito et al., 2011) techniques. Strong adsorption band of metal NPs is another quantum scale effect, which is absent in their individual atoms or bulk materials (Ghosh & Pal, 2007). This and many other optical properties of metal NPs originate from the surface plasmon resonance phenomenon (Ghosh & Pal, 2007). Au NPs with negative net charge adsorb biomolecules without attenuating their bioactivity (Hernández-Santos et al., 2002), thus, offering many potential applications as bio-labels (Liu & Lin, 2005) or enzymes immobilizing platform (Pingarrón et al., 2008). Au NPs size and surface chemistry, and consequently their optical and electrochemical properties, are easy to modify. This feature has made Au NPs one of the most widely used nanomaterials for academic research and an integral component in point-of-care medical devices and industrial products (Shumyantseva et al., 2005; Rosi & Mirkin, 2005). Solar conversion (Tian & Tatsuma, 2005), single-electron transistors (Bolotin et al., 2004), cancer diagnostics and therapy (Huang et al., 2007), optoelectronics (Willner & Willner, 2001), and quantum devices (Junno et al., 1998) are some of the examples of Au NPs applications.

MWCNTs display metallic, semi-metallic or supermetallic conductivity depending on the applied synthesis method and surface treatment. They provide a hollow core proper for immobilizing platforms, and a 1D electron confinement with a high mean free path. Consequently, MWCNTs play an important role in biomedical diagnostics as they improve the electron transfer kinetics toward the redox center of enzymes or biomolecules (Boero et al., 2011; Carrara et al., 2008, 2009). Furthermore, they find many applications in integrated circuit technology (Nihei et al., 2005), optical displays (Paddeu et al., 1998), single-electron transistors (Roschier et al., 1999), single-molecular detectors (Sorgenfrei et al., 2011), solar cells (Lin et al., 2011), and fuel cells (Prabhuram et al., 2006). MWCNTs are grown on a vast variety of substrates by means of chemical vapor deposition (Taurino et al., 2013; Singh et al., 2003), electrophoretic deposition (Boccaccini et al., 2006), arc discharge (Cadek et al., 2002), laser ablation (evaporation) (Journet & Bernier, 1998), as well as new by techniques including solar energy evaporation, plasma torch, underwater AC electric arc, and microgravity environment (Paradise & Goswami, 2007). All in all, MWCNTs with high surface to volume ratio, good mechanical properties, and great electrical conductivity improve the sensitivity, selectivity and LOD (Boero et al., 2011).

In the present work, the above-mentioned nanomaterials were used to functionalize SPEs in order to compare the performance of the resulting sensors in terms of sensitivity, LOD and redox potential toward H_2O_2 sensing.

Experimental

Materials and instrumentation

SPEs (model DRP-C110) were purchased from DropSens (Spain). Electrodes consisted of a 0.12 cm^2 carbon working electrode, a silver reference electrode and a carbon counter electrode. Suspension of dodecanethiol functionalized Au NPs, with average particle size of 4 nm and concentration of 2 mass % in toluene, was provided by Sigma–Aldrich, and diluted with toluene to obtain the density of 1 mg mL^{-1}. H_2O_2 solution was supplied by Reactolab SA (Switzerland) and diluted in phosphate buffer solution (PBS 0.01 M, pH 7.4) to provide a 25 mM solution. Powder of MWCNTs (diameter: 10 nm; length: 1–2 μm, 90 % purity) was purchased from DropSens (Spain). It was dispersed in chloroform to the concentration of 1 mg mL^{-1} and the suspension was subjected to sonication for 1 h to achieve a homogeneous solution. Bi_2O_3 NPs, synthesized in Politecnico di Torino, were dispersed in acetone to the density of 2 mg mL^{-1}, and then sonicated.

Bi_2O_3 NPs were synthesized starting from a bismuth salt (Zhao et al., 2004; Kharissova et al., 2010) following the Metal Organic Chemical Vapor Deposition (MOCVD) process (Feil et al., 1990). MOCVD was selected due to the possibility of optimizing various parameters with the scale up from a few milligrams to kilograms. The metal organic precursor was evaporated in inert atmosphere with regulated temperature so as to form metal nanoparticles. By varying the MOCVD experimental conditions, it was

possible to tailor the properties of the crystals at the atomic scale. Bismuth(III) nitrate pentahydrate ($Bi(NO_3)_3 \cdot 5H_2O$) (Aldrich, 98% purity) was used as bismuth and oxide atomic source for synthesizing Bi_2O_3 NPs.

The first step of the process was to get rid of residual air using pure argon gas flow. Then, the furnace was brought to a thermal equilibrium at the required deposition temperature (600 °C). In the furnace, the high temperature leads to the pyrolysis of the starting material, $Bi(NO_3)_3 \cdot 5H_2O$, into a gas mixture, which ultimately leads to the nanoparticle growth inside the glass vial. When the growth process ended, the furnace was allowed to cool down to ambient temperature while maintaining the inert gas flow.

A MERLIN scanning electron microscope (Carl Zeiss, Germany) was used to obtain SEM images of the nanostructures. SEM images confirmed that the surfaces of working electrodes were completely covered with nanostructures. The average diameter of Bi_2O_3 NPs (Fig. 1) was computed by the ImageJ software (Schneider et al., 2012).

Electro-active surface area

The gain of nanostructures in terms of additional electroactive surface area has widely been reported. Therefore, the aim of this work was to investigate and prove that nanostructures offer different gains in terms of sensitivity, LOD and redox potentials even if they provide equal surface area. Cottrell and Randles-Sevcik equations verify the direct relationship between the electrochemical faradaic current and the surface area of electrodes. Furthermore, it was proved (Carrara et al., 2014) that the sensitivity (S) calculated from the faradaic current versus concentration is directly related to the additional electroactive surface area (Eq. (1), where n = number of electrons, F = Faraday constant, A = electrode area, D = diffusion coefficient, t = time):

$$S = \frac{nF(A_g + A_{CNT})\sqrt{D}}{A_g\sqrt{\pi t}} \quad (1)$$

Further, the SSA of target nanostructures was approximately defined (Eqs. (2), (4)) in order to calculate the additional electroactive surface area. SPE with 100 μg of Bi_2O_3 NPs is considered as the reference (Eq. (5)), and the amounts of Au NPs and MWCNTs to achieve almost the same additional electroactive surface area were calculated (Eqs. (6), (7)).

Bi_2O_3 NPs, without taking into account their porous surface morphology, are roughly considered as spheres with the average size of 64 nm (based on SEM images in Fig. 1). SSA (area over mass in $m^2\ g^{-1}$) can be calculated for the sample using the following equation (Lowell & Shields, 1991) where $A = 4\pi r^2$, $V = 4/3\pi r^3$, $\rho = 8.9\ g\ cm^{-3}$, and $r = 32$ nm:

$$SSA_{Bi_2O_3} = \frac{A}{V\rho} = \frac{3}{r\rho} = 10.5\ m^2\ g^{-1} \quad (2)$$

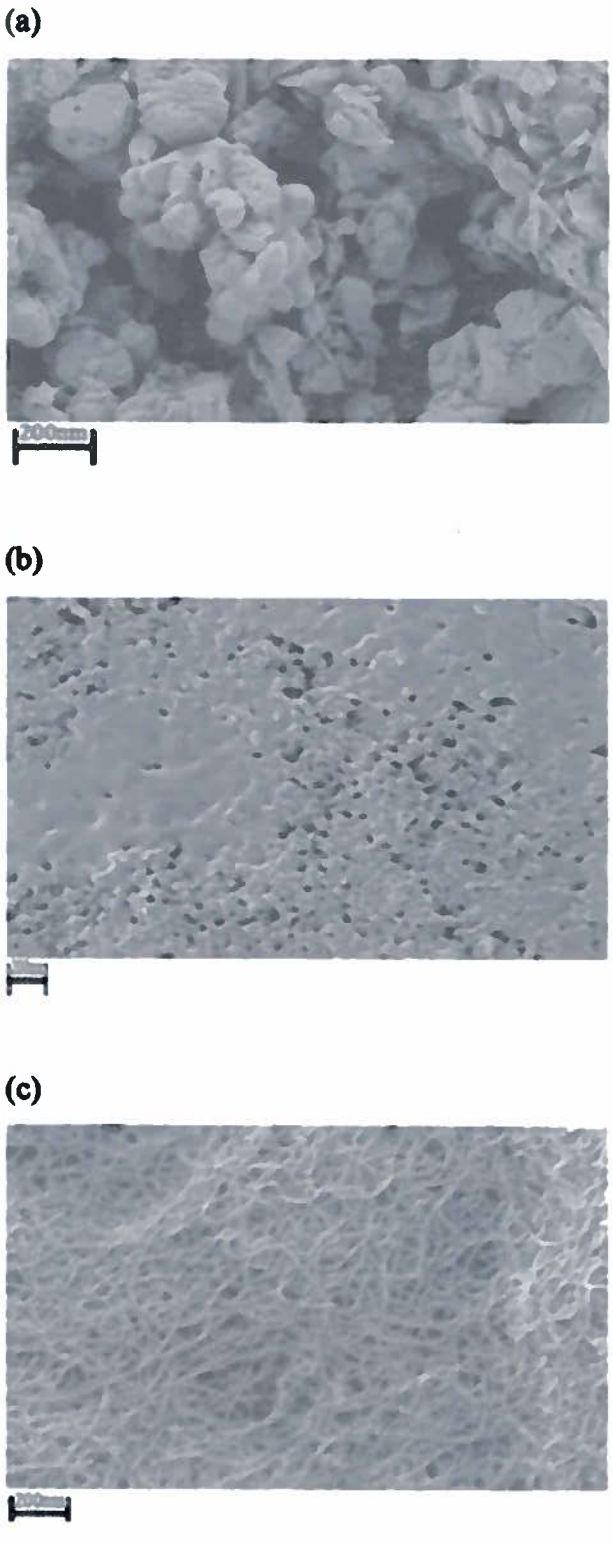

Fig. 1. SEM images of the surface of working electrodes functionalized with: Bi_2O_3 NPs (a), Au NPs (b), MWCNTs (c).

Table 1. Oxidation peak position related to nanostructured and bare SPEs for H_2O_2–25 mM sensing; additional electroactive surface area provided by the nanostructures is approximately 1050 mm^2 in respect to SPE

Working electrode[a]	SPE	MWCNTs–4.8 μg	Bi_2O_3–100 μg	Au–13.5 μg
Peak position/mV	688 ± 8	589 ± 1	790 ± 1	386 ± 1

a) Carbon–0.12 cm^2.

Au NPs also, according to the data sheets of Sigma–Aldrich and the SEM images (Fig. 1), have sphere-shaped geometry with average dimensions of 4 nm. The SSA_{Au} of 77.7 $m^2\ g^{-1}$ was calculated using Eq. (2), where $r = 2$ nm and $\rho = 19.3\ g\ cm^{-3}$. SSA of MWCNTs was calculated according to Eq. (3a) (Peigney et al., 2001), where d_e is the MWCNTs diameter (10 nm), $d_{s\text{-}s}$ is the inter-shell distance (0.34 nm), SSA_{GS} is the SSA of one side of a graphene sheet (1315 $m^2\ g^{-1}$), and n is the number of shells (calculated according to Eq. (3b) following the work of Haruehanroengra and Wang (2007)).

$$SSA_{MWCNTs} = \frac{S_{MW}}{W_{MW}} = \frac{SSA_{GS} d_e}{n d_e - 2 d_{s\text{-}s}\left[\sum_{i=1}^{n-1} i\right]} \quad (3a)$$

$$n = 1 + \frac{d_e}{4 d_{s\text{-}s}} = 8 \quad (3b)$$

Consequently, SSA_{MWCNTs} for the sample used in this work can be calculated as:

$$SSA_{MWCNT} = \frac{1315 d_e}{n d_e - 0.68\left[\sum_{i=1}^{n-1} i\right]} = 215.7\ m^2 g^{-1} \quad (4)$$

In the next step, the amount of additional electroactive surface area with 100 μg of Bi_2O_3 was evaluated, and used as reference:

$$\left(100 \times 10^{-6}\right)\left(SSA_{Bi_2O_3}\right) = \\ = \left(100 \times 10^{-6} g\right)\left(10.5\ m^2 g^{-1}\right) = 1050\ mm^2 \quad (5)$$

The amount of Au NPs and MWCNTs for the deposition was calculated according to Eqs. (6) and (7), respectively.

$$1050\ mm^2 = X_{Au} SSA_{Au} \Rightarrow \\ 1050\ mm^2 = X_{Au}(19.3\ m^2\ g^{-1}) \Rightarrow \\ X_{Au} = 13.5\ \mu g \quad (6)$$

$$1050\ mm^2 = X_{MWCNTs} SSA_{MWCNTs} \Rightarrow \\ 1050\ mm^2 = X_{MWCNTs}(215.7\ m^2\ g^{-1}) \Rightarrow \\ X_{MWCNTs} = 4.8\ \mu g \quad (7)$$

SPEs were covered with the amount of nanostructures based on the above-mentioned values, and they are referred as Bi_2O_3–100 μg, Au–13.5 μg, and MWCNTs–4.8 μg.

Electrode preparation and electrochemical experiments

Sensing elements were prepared by the drop casting technique (Shumyantseva et al., 2005) as follows: 50 μL of Bi_2O_3 NPs suspension (in 5 μL steps), 4.8 μL of MWCNTs suspension (in 0.8 μL steps), and 13.5 μL of Au NPs suspension (four steps of 3 μL and one step of 1.5 μL) were deposited, and allowed to dry after each deposition step. Electrodes were stored at ambient temperature after the deposition (Guascito et al., 2011).

Electrochemical measurements (CA and CV) were performed under aerobic conditions using AutoLab potensiostat/galvanostat and functionalized electrodes as sensing elements. To obtain the voltammograms, surface of the working electrode of the sensor was covered with 100 μL of a 25 mM H_2O_2 solution (H_2O_2–25 mM). Then, the device was configured to sweep the voltage in the range of −1 to +1 V (versus Ag) with the scan rate of 100 mV s^{-1}. The peak positions of voltammograms (data in Table 1) were assessed by curve fitting using the IGOR Pro software (Wavemetrics, Lake Oswego, OR, USA). The best fit of the voltammogram shapes was obtained when constant baseline and Gaussians were used (Sadezky et al., 2005).

For CA, the electrodes were immersed in 10 mL of PBS (0.1 M, pH 7.4) in which H_2O_2 was injected in steps of 100 μM until the total amount of 500 μM was achieved. The applied potential was set slightly above the oxidation peak obtained from the voltammogram analysis. To achieve better evaluation: four SPEs were functionalized with one type of nanostructure and tested using CA. Then, the calibration curves were evaluated after removing the blank measurements from the data obtained. In the next step, the slope of the calibration curve was divided by surface area of the working electrode to identify the normalized sensitivity. Standard deviations were calculated using Excel. LOD was calculated using Eq. (7) (Mocak et al., 1997), where ΔD is the standard deviation of blank measurements, S is the sensitivity, and K is a parameter accounting for the confidence level (K = 1, 2, or 3 corresponding to 68.2 %, 95.4 %, or 99.6 % of statistical confidence, respectively). Finally, results obtained from the four SPEs were averaged to get the sensitivity, and LOD corresponding to the nanostructure. This procedure was repeated for every nanos-

Table 2. CA results to compare sensitivity and LODs of tested electrodes for H_2O_2 detection. Additional electroactive surface area provided by nanostructures is approximately 1050 mm^2 with respect to SPE

Working electrode[a]	SPE	MWCNTs–4.8 μg	Bi_2O_3–100 μg	Au–13.5 μg
Sensitivity/μA	40 ± 5	54 ± 2	74 ± 12	129 ± 15
LODs/μM	11.3 ± 2.1	3.4 ± 0.1	11.1 ± 2.8	8.0 ± 2.4
Potential/mV	750 ± 2	620 ± 1	850 ± 2	450 ± 1

a) Carbon–0.12 cm^2.

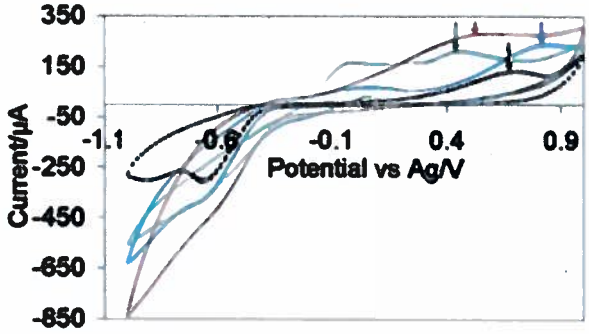

Fig. 2. CV response of nanostructures for the detection of H_2O_2–25 mM: Bi_2O_3–100 μg (blue curve), MWCNTs–4.8 μg (brown curve), Au–13.5 μg (green curve), and bare SPE (black dotted curve). Potential sweep: –1 and +1 V (versus Ag), scan rate: 100 mV s^{-1}. Peak positions are pointed by arrows.

tructure and the results are summarized in Table 2.

$$\mathrm{LOD} = \frac{K\Delta D}{S} \tag{8}$$

Results and discussion

Cyclic voltammetry

Nanostructured electrodes were tested using CV under the same experimental conditions as those applied to detect H_2O_2–25 mM. The acquired voltammograms are shown in Fig. 2. A clearly detectable oxidation peak can be observed for Au–13.5 μg at 386 mV, which is lower than 589 mV and 790 mV found with MWCNTs–4.8 μg and for Bi_2O_3–100 μg, respectively. Oxidation peak positions in Table 1 show a negative shift of 302 mV and 99 mV for Au NPs, and MWCNTs, in respect to SPE, while a positive shift of 102 mV for Bi_2O_3 NPs can be observed.

The peak positions for fully-irreversible systems in thin layer models were proposed by Hubbard (1969). Further, Streeter et al. (2008) described that in case of nanostructuring, the semi-infinite planar diffusion is not applicable, and the peak positions should be described by a thin layer model. The following Eq. (9) (where E_f is the formal electrode potential and l is the thickness of the thin layer) defines the peak positions of such a system in CV:

$$E_p = E_f \frac{RT}{\alpha F} \ln\left(\frac{\alpha F \nu}{RTlk_0}\right) \tag{9}$$

As l decreases, the amount of electroactive species trapped inside the thin layer is reduced, and thus, the layer depletion is faster. This means that redox peaks shift toward lower values. Carrara et al. (2014) reported CV responses of some MWCNT-based electrodes not obeying this thin layer model (layering effect). For example, ferricyanide, and etoposide did not show any layering effect, and ifosfamide opposed it when metabolized by CYP450-3A4.

In this work it is demonstrated that Au–13.5 μg and MWCNTs–4.8 μg conform to the layering effect with an almost 300 mV and 100 mV negative shift of the oxidation peak, while Bi_2O_3–100 μg opposes it with a 100 mV positive shift. The same behavior was reported in literature. For instance, Yin et al. (2009) and Yang et al. (2008) reported an approximately 100 mV and 50 mV negative shift of the redox peak in H_2O_2 detection after applying Au NPs. Moreover, Hu et al. (2008) demonstrated that Au nanostructuring decreases the ascorbic acid (AA) redox peak (345 mV) while the peak of uric acid (UA) was not affected at all. Considering MWCNTs, a 100 mV negative shift of the H_2O_2 redox peak was observed in the work by Woo et al. (2012). Also, Habibi and Pournaghi-Azar (2010) reported 348 mV, 374 mV, and 450 mV negative shifts regarding the DA, AA, and UA redox peaks, respectively. To the best of our knowledge, there is not that much work on the electrochemical behavior of Bi_2O_3 NPs against H_2O_2 published. Nevertheless, an approximately 100 mV positive shift was observed by Taufik et al. (2011) when using Bi_2O_3 NPs in a DNA biosensor.

Various shifts reported in literature for a specific nanostructure are probably caused by the difference in the electrode preparation techniques (different working electrodes, size of nanoparticles, additional electroactive surface area, etc.). For example, at a 500 mV negative shift of the H_2O_2 redox peak with MWCNTs nanostructuring was reported (Carrara et al., 2014), this value is five-fold higher than that reported here (100 mV). This is due to the difference in the amount of deposited nanostructures, since an almost six-fold (30 μg) of MWCNTs was used compared to this work

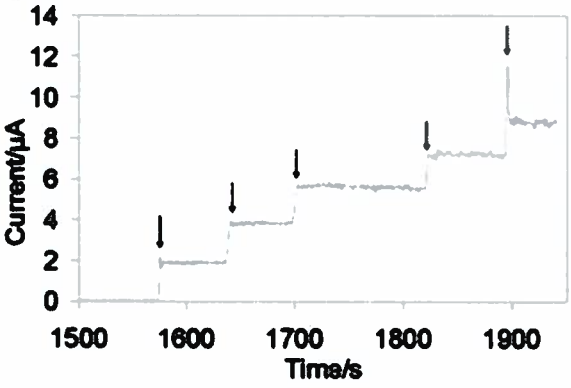

Fig. 3. CA response to Au–13.5 μg. Injections of 100 μM H_2O_2 are pointed out by arrows.

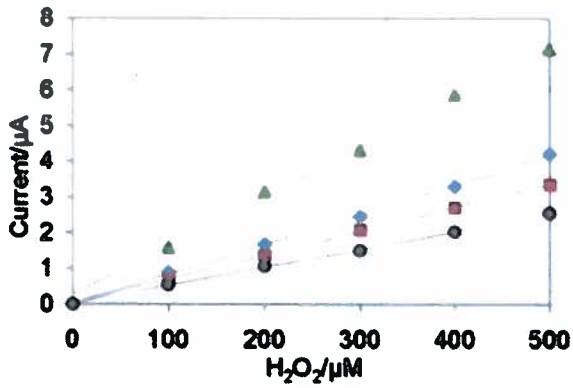

Fig. 4. Calibration curves obtained by analyzing the CA response of the nanostructured electrodes: Bi_2O_3–100 μg (◆), MWCNTs–4.8 μg (■), Au–13.5 μg (▲), and bare SPE (●). Slope of the lines identifies the sensitivity related to each nanostructure.

(4.8 μg). The present work and the above mentioned examples prove that CV responses of sensors are not influenced only by the additional electroactive surface but that to analyze and predict their electrochemical behavior, a combination of elements, including bare electrodes, nanostructures, immobilized enzymes, and target molecules should be considered.

Chronoamperometry

CA was carried out for Bi_2O_3–100 μg, Au–13.5 μg, and MWCNTs–4.8 μg at 850 mV, 450 mV, and 620 mV, respectively. In addition, bare SPE was examined by CA with the applied potential of 750 mV as a reference. H_2O_2 was injected in PBS (pH 7.4) by 100 μM steps in the range of 0–500 μM. The system gave a clear step response after each injection with the amplitude directly related to the concentration of H_2O_2 (Fig. 3). Therefore, steps related to each injection were averaged and converted to points in the calibration curve shown in Fig. 4. Standard deviations were calculated for each step and they are presented in the figure as error bars. Blank measurement or noise of the system were averaged and removed from the data for higher precision (Mocak et al., 1997). Calibration curve of Au NPs in Fig. 4 shows a steeper slope than the other curves as Au NPs enhanced the sensitivity compared to reference bare SPE, while Bi_2O_3 NPs and MWCNTs show lower improvement.

Quantitative values of sensitivity and LOD in Table 2 present an improvement by one order of magnitude improvement in the Au NPs sensitivity. Many studies have reported enhancement achieved by using Au NPs. For instance, Li et al. (2008) presented sensitivity increment by comparing calibration curves of their electrodes for H_2O_2 detection with and without Au NPs. However, only a few works on non-enzymatic detection of H_2O_2 with Au NPs based electrodes have been published. In this work, the sensitivity of electrodes to H_2O_2 increased more than three-fold compared to a bare carbon electrode. On the other hand, MWCNTs and Bi_2O_3 NPs based electrodes showed sensitivity increment of almost 1.5-fold. It is important to consider that all the experimental conditions and configurations are the same except for the dimensions of Au NPs. The increment in sensitivity with the decreasing dimensions of Au NPs has also been reported (German et al., 2012). The authors proved an enhancement of the amperometric response (I_{max}) in a glucose detection system by decreasing the size of Au NPs from 13 nm to 6 nm and then to 3.5 nm (66.2 μA, 73.8 μA, and 76.2 μA, respectively). This work proves the qualitative effect of dimensions on the electrochemical performance, but further investigation to achieve deeper and more quantitative knowledge is needed.

It should be mention that the decrease in LOD with the increasing sensitivity, which was expected (Carrara et al., 2014) based on Eq. (7), was not observed probably due to the noise of the system outweighting the effect of sensitivity.

Conclusions

CA and CV performed on Bi_2O_3 NPs, Au NPs, and MWCNTs based SPEs demonstrated different sensitivity, LODs and peak positions despite the fact that the same electroactive area is added. These findings prove that there are also some other factors contributing to the electrochemical behavior of nanostructures. Physical properties of the surface (such as the level of porosity and defects), the layering effect, and size dependent properties such as quantum effects are some of these factors.

The latter factor is more interesting since the electrodes functionalized with Au NPs, with dimensions under the limit of 10 nm (quantum dots), exhibit the best performance. Further works planned in our laboratory will be focused on the verification of the role of quantum phenomena on the improved sensors performance.

Acknowledgements. This research was supported by the project PROSENSE funded by the European Union's Horizon 2020 research and innovation programme under the grant agreement no 317420.

References

Alivisatos, A. P. (1996). Perspectives on the physical chemistry of semiconductor nanocrystals. *The Journal of Physical Chemistry, 100*, 13226–13239. DOI: 10.1021/jp9535506.

Banks, C. E., Davies, T. J., Wildgoose, G. G., & Compton, R. G. (2005). Electrocatalysis at graphite and carbon nanotube modified electrodes: edge-plane sites and tube ends are the reactive sites. *Chemical Communications, 2005*, 829–841. DOI: 10.1039/b413177k.

Boccaccini, A. R., Cho, J., Roether, J. A., Thomas, B. J. C., Minay, E. J., & Shaffer, M. S. P. (2006). Electrophoretic deposition of carbon nanotubes. *Carbon, 44*, 3149–3160. DOI: 10.1016/j.carbon.2006.06.021.

Boero, C., Carrara, S., Del Vecchio, G., Calzà, L., & De Micheli, G. (2011). Highly sensitive carbon nanotube-based sensing for lactate and glucose monitoring in cell culture. *IEEE Transactions on Nanobioscience, 10*, 59–67. DOI: 10.1109/tnb.2011.2138157.

Bolotin, K. I., Kuemmeth, F., Pasupathy, A. N., & Ralph, D. C. (2004). Metal-nanoparticle single-electron transistors fabricated using electromigration. *Applied Physics Letters, 84*, 3154–3156. DOI: 10.1063/1.1695203.

Bredol, M., & Kaczmarek, M. (2010). Potential of nano-ZnS as electrocatalyst. *The Journal of Physical Chemistry A, 114*, 3950–3955. DOI: 10.1021/jp907369f.

Cadek, M., Murphy, R., McCarthy, B., Drury, A., Lahr, B., Barklie, R. C., In het Panhuis, M., Coleman, J. N., & Blau, W. J. (2002). Optimisation of the arc-discharge production of multi-walled carbon nanotubes. *Carbon, 40*, 923–928. DOI: 10.1016/s0008-6223(01)00221-4.

Carrara, S., Shumyantseva, V. V., Archakov, A. I., & Samorì, B. (2008). Screen-printed electrodes based on carbon nanotubes and cytochrome P450scc for highly sensitive cholesterol biosensors. *Biosensors & Bioelectronics, 24*, 148–150. DOI: 10.1016/j.bios.2008.03.008.

Carrara, S., Boero, C., & De Micheli, G. (2009). Quantum dots and wires to improve enzymes-based electrochemical biosensing. In A. Schmid, S. Goel, W. Wang, V. Beiu, & S. Carrara (Eds.), *Nano-net: Lecture notes of the Institute for Computer Sciences, Social Informatics and Telecommunications Engineering* (Vol. *20*, pp. 189–199). Berlin, Germany: Springer. DOI: 10.1007/978-3-642-04850-0_26.

Carrara, S., Baj-Rossi, C., Boero, C., & De Micheli, G. (2014). Do carbon nanotubes contribute to electrochemical biosensing? *Electrochimica Acta, 128*, 102–112. DOI: 10.1016/j.electacta.2013.12.123.

Ding, Y., Dong, Y., Bapat, A., Nowak, J. D., Carter, C. B., Kortshagen, U. R., & Campbell, S. A. (2006). Single nanoparticle semiconductor devices. *IEEE Transactions on Electron Devices, 53*, 2525–2531. DOI: 10.1109/ted.2006.882047.

Facci, P., Erokhin, V., Carrara, S., & Nicolini, C. (1996). Room-temperature single-electron junction. *Proceedings of the National Academy of Sciences of the United States of America, 93*, 10556–10559. DOI: 10.1073/pnas.93.20.10556.

Feil, W. A., Wessels, B. W., Tonge, L. M., & Marks, T. J. (1990). Organometallic chemical vapor deposition of strontium titanate. *Journal of Applied Physics, 67*, 3858–3861. DOI: 10.1063/1.345034.

Ge, M., Li, Y., Liu, L., Zhou, Z., & Chen, W. (2011). Bi_2O_3–Bi_2WO_6 composite microspheres: Hydrothermal synthesis and photocatalytic performances. *The Journal of Physical Chemistry C, 115*, 5220–5225. DOI: 10.1021/jp108414e.

German, N., Ramanavicius, A., Voronovic, J., & Ramanaviciene, A. (2012). Glucose biosensor based on glucose oxidase and gold nanoparticles of different sizes covered by polypyrrole layer. *Colloids and Surfaces A: Physicochemical and Engineering Aspects, 413*, 224–230. DOI: 10.1016/j.colsurfa.2012.02.012.

Ghosh, S. K., & Pal, T. (2007). Interparticle coupling effect on the surface plasmon resonance of gold nanoparticles: From theory to applications. *Chemical Reviews, 107*, 4797–4862. DOI: 10.1021/cr0680282.

Guascito, M. R., Chirizzi, D., Picca, R. A., Mazzotta, E., & Malitesta, C. (2011). Ag nanoparticles capped by a non-toxic polymer: Electrochemical and spectroscopic characterization of a novel nanomaterial for glucose detection. *Materials Science and Engineering C, 31*, 606–611. DOI: 10.1016/j.msec.2010.11.022.

Guo, F., He, J., Li, J., Wu, W., Hang, Y., & Hua, J. (2013). Photovoltaic performance of bithiazole-bridged dyes-sensitized solar cells employing semiconducting quantum dot $CuInS_2$ as barrier layer material. *Journal of Colloid and Interface Science, 408*, 59–65. DOI: 10.1016/j.jcis.2013.06.069.

Habibi, B., & Pournaghi-Azar, M. H. (2010). Simultaneous determination of ascorbic acid, dopamine and uric acid by use of a MWCNT modified carbon-ceramic electrode and differential pulse voltammetry. *Electrochimica Acta, 55*, 5492–5498. DOI: 10.1016/j.electacta.2010.04.052.

Haruehanroengra, S., & Wang, W. (2007). Analyzing conductance of mixed carbon-nanotube bundles for interconnect applications. *IEEE Electron Device Letters, 28*, 756–759. DOI: 10.1109/led.2007.901584.

Hernández-Santos, D., González-García, M. B., & García, A. C. (2002). Metal-nanoparticles based electroanalysis. *Electroanalysis, 14*, 1225–1235. DOI: 10.1002/1521-4109(200210)14:18<1225::AID-ELAN1225>3.0.CO;2-Z.

Hu, G., Ma, Y., Guo, Y., & Shao, S. (2008). Electrocatalytic oxidation and simultaneous determination of uric acid and ascorbic acid on the gold nanoparticles-modified glassy carbon electrode. *Electrochimica Acta, 53*, 6610–6615. DOI: 10.1016/j.electacta.2008.04.054.

Huang, X., Jain, P. K., El-Sayed, I. H., & El-Sayed, M. A. (2007). Gold nanoparticles: interesting optical properties and recent applications in cancer diagnostics and therapy. *Nanomedicine, 2*, 681–693. DOI: 10.2217/17435889.2.5.681.

Hubbard, A. T. (1969). Study of the kinetics of electrochemical reactions by thin-layer voltammetry: I. theory. *Journal of Electroanalytical Chemistry and Interfacial Electrochemistry, 22*, 165–174. DOI: 10.1016/s0022-0728(69)80247-0.

Jiang, L., You, T., & Deng, W. Q. (2013). Enhanced photovoltaic performance of a quantum dot-sensitized solar cell using a Nb-doped TiO_2 electrode. *Nanotechnology, 24*, 415401. DOI: 10.1088/0957-4484/24/41/415401.

Journet, C., & Bernier, P. (1998). Production of carbon nanotubes. *Applied Physics A: Materials Science & Processing, 67*, 1–9. DOI: 10.1007/s003390050731.

Junno, T., Carlsson, S. B., Xu, H., Montelius, L., & Samuelson, L. (1998). Fabrication of quantum devices by Ångström-level manipulation of nanoparticles with an atomic force microscope. *Applied Physics Letters, 72*, 548–550. DOI: 10.1063/1.120754.

Kairdolf, B. A., Smith, A. M., Stokes, T. H., Wang, M. D., Young, A. N., & Nie, S. (2013). Semiconductor quantum dots for bioimaging and biodiagnostic applications. *Annual Review of Analytical Chemistry, 6*, 143–162. DOI: 10.1146/annurev-anchem-060908-155136.

Kharissova, O. V., Osorio, M., Kharisov, B. I., Yacamán, M. J., & Méndez, U. O. (2010). A comparison of bismuth nanoforms obtained in vacuum and air by microwave heating of bis-

muth powder. *Materials Chemistry and Physics*, *121*, 489–496. DOI: 10.1016/j.matchemphys.2010.02.013.

Li, N. B., Park, J. H., Park, K., Kwon, S. J., Shin, H., & Kwak, J. (2008). Characterization and electrocatalytic properties of Prussian blue electrochemically deposited on nano-Au/PAMAM dendrimer-modified gold electrode. *Biosensors & Bioelectronics*, *23*, 1519–1526. DOI: 10.1016/j.bios.2008.01.009.

Lin, J. Y., Liao, J. H., & Hung, T. Y. (2011). A composite counter electrode of CoS/MWCNT with high electrocatalytic activity for dye-sensitized solar cells. *Electrochemistry Communications*, *13*, 977–980. DOI: 10.1016/j.elecom.2011.06.016.

Liu, G., & Lin, Y. (2005). A renewable electrochemical magnetic immunosensor based on gold nanoparticle labels. *Journal of Nanoscience and Nanotechnology*, *5*, 1060–1065. DOI: 10.1166/jnn.2005.178.

Liu, B., Wang, Z., Dong, Y., Zhu, Y., Gong, Y., Ran, S., Liu, Z., Xu, J., Xie, Z., Chen, D., & Shen, G. (2012). ZnO-nanoparticle-assembled cloth for flexible photodetectors and recyclable photocatalysts. *Journal of Materials Chemistry*, *22*, 9379-9384. DOI: 10.1039/c2jm16781f.

Lowell, S., & Shields, J. E. (1991). *Powder surface area and porosity* (3rd ed.). London, UK: Chapman and Hall.

Mocak, J., Bond, A. M., Mitchell, S., & Scollary, G. (1997). A statistical overview of standard (IUPAC and ACS) and new procedures for determining the limits of detection and quantification: Application to voltammetric and stripping techniques. *Pure and Applied Chemistry*, *69*, 297–328. DOI: 10.1351/pac199769020297.

Nie, Z., Petukhova, A., & Kumacheva, E. (2010). Properties and emerging applications of self-assembled structures made from inorganic nanoparticles. *Nature Nanotechnology*, *5*, 15–25. DOI: 10.1038/nnano.2009.453.

Nihei, M., Kondo, D., Kawabata, A., Sato, S., Shioya, H., Sakaue, M., Iwai, T., Ohfuti, M., & Awano, Y. (2005). Low-resistance multi-walled carbon nanotube vias with parallel channel conduction of inner shells. *Proceedings of the IEEE 2005 International Interconnect Technology Conference*, June 6–8, 2005 (pp. 234–236). Burlingame, CA, USA: IEEE *Xplore*. DOI: 10.1109/iitc.2005.1499995.

Paddeu, S., Ram, M. K., Carrara, S., & Nicolini, C. (1998). Langmuir–Schaefer films of a poly(o-anisidine) conducting polymer for sensors and displays. *Nanotechnology*, *9*, 228–236. DOI: 10.1088/0957-4484/9/3/014.

Paradise, M., & Goswami, T. (2007). Carbon nanotubes – Production and industrial applications. *Materials & Design*, *28*, 1477–1489. DOI: 10.1016/j.matdes.2006.03.008.

Peigney, A., Laurent, C., Flahaut, E., Bacsa, R. R., & Rousset, A. (2001). Specific surface area of carbon nanotubes and bundles of carbon nanotubes. *Carbon*, *39*, 507–514. DOI: 10.1016/s0008-6223(00)00155-x.

Periasamy, A. P., Yang, S., & Chen, S. M. (2011). Preparation and characterization of bismuth oxide nanoparticles-multiwalled carbon nanotube composite for the development of horseradish peroxidase based H_2O_2 biosensor. *Talanta*, *87*, 15–23. DOI: 10.1016/j.talanta.2011.09.021.

Pingarrón, J. M., Yáñez-Sedeño, P., & González-Cortés, A. (2008). Gold nanoparticle-based electrochemical biosensors. *Electrochimica Acta*, *53*, 5848–5866. DOI: 10.1016/j.electacta.2008.03.005.

Prabhuram, J., Zhao, T. S., Tang, Z. K., Chen, R., & Liang, Z. X. (2006). Multiwalled carbon nanotube supported PtRu for the anode of direct methanol fuel cells. *The Journal of Physical Chemistry B*, *110*, 5245–5252. DOI: 10.1021/jp0567063.

Pumera, M., Sánchez, S., Ichinose, I., & Tang, J. (2007). Electrochemical nanobiosensors. *Sensors and Actuators B: Chemical*, *123*, 1195–1205. DOI: 10.1016/j.snb.2006.11.016.

Roschier, L., Penttilä, J., Martin, M., Hakonen, P., Paalanen, M., Tapper, U., Kauppinen, E. I., Journet, C., & Bernier, P. (1999). Single-electron transistor made of multiwalled carbon nanotube using scanning probe manipulation. *Applied Physics Letters*, *75*, 728–730. DOI: 10.1063/1.124495.

Rosi, N. L., & Mirkin, C. A. (2005). Nanostructures in biodiagnostics. *Chemical Reviews*, *105*, 1547–1562. DOI: 10.1021/cr030067f.

Sadezky, A., Muckenhuber, H., Grothe, H., Niessner, R., & Pöschl, U. (2005). Raman microspectroscopy of soot and related carbonaceous materials: Spectral analysis and structural information. *Carbon*, *43*, 1731–1742. DOI: 10.1016/j.carbon.2005.02.018.

Schneider, C. A., Rasband, W. S., & Eliceiri, K. W. (2012). NIH Image to ImageJ: 25 years of image analysis. *Nature Methods*, *9*, 671–675. DOI: 10.1038/nmeth.2089.

Shipway, A. N., & Willner, I. (2001). Nanoparticles as structural and functional units in surface-confined architectures. *Chemical Communications*, *2001*, 2035–2045. DOI: 10.1039/b105164b.

Shumyantseva, V. V., Carrara, S., Bavastrello, V., Riley, D. J., Bulko, T. V., Skryabin, K. G., Archakov, A. I., & Nicolini, C. (2005). Direct electron transfer between cytochrome P450scc and gold nanoparticles on screen-printed rhodium–graphite electrodes. *Biosensors & Bioelectronics*, *21*, 217–222. DOI: 10.1016/j.bios.2004.10.008.

Singh, C., Shaffer, M. S. P., & Windle, A. H. (2003). Production of controlled architectures of aligned carbon nanotubes by an injection chemical vapour deposition method. *Carbon*, *41*, 359–368. DOI: 10.1016/s0008-6223(02)00314-7.

Sorgenfrei, S., Chiu, C. Y., Gonzalez, R. L., Jr., Yu, Y. J., Kim, P., Nuckolls, C., & Shepard, K. L. (2011). Label-free single-molecule detection of DNA-hybridization kinetics with a carbon nanotube field-effect transistor. *Nature Nanotechnology*, *6*, 126–132. DOI: 10.1038/nnano.2010.275.

Streeter, I., Wildgoose, G. G., Shao, L., & Compton, R. G. (2008). Cyclic voltammetry on electrode surfaces covered with porous layers: An analysis of electron transfer kinetics at single-walled carbon nanotube modified electrodes. *Sensors and Actuators B: Chemical*, *133*, 462–466. DOI: 10.1016/j.snb.2008.03.015.

Sun, S. (2006). Recent advances in chemical synthesis, self-assembly, and applications of FePt nanoparticles. *Advanced Materials*, *18*, 393–403. DOI: 10.1002/adma.200501464.

Taufik, S., Yusof, N. A., Tee, T. W., & Ramli, I. (2011). Bismuth oxide nanoparticles/chitosan/modified electrode as biosensor for DNA hybridization. *International Journal of Electrochemical Science*, *6*, 1880–1891.

Taurino, I., Magrez, A., Matteini, F., Forró, L., De Micheli, G., & Carrara, S. (2013). Direct growth of nanotubes and graphene nanoflowers on electrochemical platinum electrodes. *Nanoscale*, *5*, 12448–12455. DOI: 10.1039/c3nr03283c.

Tian, Y., & Tatsuma, T. (2005). Mechanisms and applications of plasmon-induced charge separation at TiO_2 films loaded with gold nanoparticles. *Journal of the American Chemical Society*, *127*, 7632–7637. DOI: 10.1021/ja042192u.

Trindade, T., O'Brien, P., & Pickett, N. L. (2001). Nanocrystalline semiconductors: Synthesis, properties, and perspectives. *Chemistry of Materials*, *13*, 3843–3858. DOI: 10.1021/cm000843p.

Wang, F., & Hu, S. (2009). Electrochemical sensors based on metal and semiconductor nanoparticles. *Microchimica Acta*, *165*, 1–22. DOI: 10.1007/s00604-009-0136-4.

Wang, Q., & Zheng, J. (2010). Electrodeposition of silver nanoparticles on a zinc oxide film: improvement of amperometric sensing sensitivity and stability for hydrogen perox-

ide determination. *Microchimica Acta*, *169*, 361–365. DOI: 10.1007/s00604-010-0356-7.

Willner, I., & Willner, B. (2001). Molecular and biomolecular optoelectronics. *Pure and Applied Chemistry*, *73*, 535–542.

Willner, I., Baron, R., & Willner, B. (2007). Integrated nanoparticle–biomolecule systems for biosensing and bioelectronics. *Biosensors & Bioelectronics*, *22*, 1841–1852. DOI: 10.1016/j.bios.2006.09.018.

Woo, S., Kim, Y. R., Chung, T. D., Piao, Y., & Kim, H. (2012). Synthesis of a graphene–carbon nanotube composite and its electrochemical sensing of hydrogen peroxide. *Electrochimica Acta*, *59*, 509–514. DOI: 10.1016/j.electacta.2011.11.012.

Yang, G., Yuan, R., & Chai, Y. Q. (2008). A high-sensitive amperometric hydrogen peroxide biosensor based on the immobilization of hemoglobin on gold colloid/L-cysteine/gold colloid/nanoparticles Pt–chitosan composite film-modified platinum disk electrode. *Colloids and Surfaces B: Biointerfaces*, *61*, 93–100. DOI: 10.1016/j.colsurfb.2007.07.014.

Yin, H., Ai, S., Shi, W., & Zhu, L. (2009). A novel hydrogen peroxide biosensor based on horseradish peroxidase immobilized on gold nanoparticles–silk fibroin modified glassy carbon electrode and direct electrochemistry of horseradish peroxidase. *Sensors and Actuators B: Chemical*, *137*, 747–753. DOI: 10.1016/j.snb.2008.12.046.

Yin, G., Xing, L., Ma, X. J., & Wan, J. (2014). Non-enzymatic hydrogen peroxide sensor based on a nanoporous gold electrode modified with platinum nanoparticles. *Chemical Papers*, *68*, 435–441. DOI: 10.2478/s11696-013-0473-y.

Zeng, H., Duan, G., Li, Y., Yang, S., Xu, X., & Cai, W. (2010). Blue luminescence of ZnO nanoparticles based on non-equilibrium processes: Defect origins and emission controls. *Advanced Functional Materials*, *20*, 561–572. DOI: 10.1002/adfm.200901884.

Zhang, J. Z. (1997). Ultrafast studies of electron dynamics in semiconductor and metal colloidal nanoparticles: Effects of size and surface. *Accounts of Chemical Research*, *30*, 423–429. DOI: 10.1021/ar960178j.

Zhang, H., Wu, P., Li, Y., Liao, L., Fang, Z., & Zhong, X. (2010). Preparation of bismuth oxide quantum dots and their photocatalytic activity in a homogeneous system. *ChemCatChem*, *2*, 1115–1121. DOI: 10.1002/cctc.201000090.

Zhao, Y., Zhang, Z., & Dang, H. (2004). A simple way to prepare bismuth nanoparticles. *Materials Letters*, *58*, 790–793. DOI: 10.1016/j.matlet.2003.07.013.